Supporting Information for "Electron Acceptors Promote Proton-Hydride Tautomerism in Low Valent Rhenium β-Diketiminates"

Trevor D. Lohrey,[a,b] Jade I. Fostvedt,[a] Robert G. Bergman,[a,*] and John Arnold[a,b,*]

[a] Department of Chemistry, University of California, Berkeley, CA, United States

[b] Chemical Sciences Division, Lawrence Berkeley National Laboratory, Berkeley, CA, United States

Table of Contents:

General Considerations

All manipulations were carried out under a dry nitrogen atmosphere, either in an MBraun LabStar glovebox or on a Schlenk line using standard techniques. Toluene, diethyl ether, and tetrahydrofuran were dried by passage through a basic alumina column and were handled and stored under a dry nitrogen atmosphere in standard Strauss flasks or in the glovebox. Hexamethyldisiloxane (HMDSO) was dried over Na/benzophenone, distilled under N_2, and stored in the glovebox prior to use. Deuterated benzene was obtained commercially, dried over an appropriate reagent (Na/benzophenone), and distilled prior to storage in the glovebox over molecular sieves. Celite was dried in a 150 °C oven for 24 hours prior to storage in the glovebox. 2,6-di-*tert*-butylphenol was obtained commercially and purified by sublimation prior to storage in the glovebox. Carbon monoxide was obtained commercially and handled exclusively inside a fume hood. The reported compounds Na[Re(η^5-Cp)(BDI)],[1] {(Et_2O)Na[(OC)Re(η^5-Cp)(BDI)]}$_2$,[2] triethylammonium tetraphenylborate[3] (and its deuterated analog), and 2,6-xylylisocyanide,[4] were synthesized using known procedures. Unless noted otherwise, "room temperature" and "ambient temperature" both refer to approx. 23 °C. NMR spectroscopy data were obtained on Bruker AV-500 and AV-600 instruments. All ^{1}H and ^{13}C spectra were referenced to the residual peak of the solvent used. Select peak assignments were corroborated with ^{1}H-^{13}C HSQC experiments as necessary. FT-IR data were obtained using a Thermo Scientific Nicolet iS10 instrument, with the sample chamber under ambient atmosphere. FT-IR samples were prepared as Nujol mulls pressed between KBr plates in the glovebox.

Synthetic Procedures

(CO)Re(η^5-Cp)(BDI-H) (1-CO)

{(Et_2O)Na[(OC)Re(η^5-Cp)(BDI)]}$_2$ (50 mg, 0.031 mmol) was dissolved in THF (4 mL) and this solution was set to stir. Separately, triethylammonium tetraphenylborate (27 mg, 0.063 mmol) was dissolved in THF (4 mL) and this solution was added to the green solution of rhenium carbonyl by pipette, leading to an immediate color change to bright red. After the reaction mixture was stirred for 15 minutes, its volatile components were removed in vacuo. The dry residue was extracted with toluene (6 mL), and these extracts were filtered through Celite. The volatile components of the filtered extracts were removed in vacuo to give a red crystalline residue, which was washed with Et_2O (2 x 2 mL) before removing the residual solvent in vacuo to yield **1-CO** (35 mg, 80%). m.p.: decomp. 160-168 °C without melting. ^{1}H NMR for **2-CO** (600 MHz, C_6D_6, 298 K): 7.11 (d, 2H, *J* = 5.1 Hz, BDI Ar), 7.04 (bs, 4H, BDI Ar), 4.68 (s, 1H, *H*C[MeC(NAr)]$_2$), 4.14 (s, 5H, Cp), 3.77 (bs, 1H, BDI C*H*(Me)$_2$), 3.66 (bs, 1H, BDI C*H*(Me)$_2$), 3.56 (bs, 1H, BDI C*H*(Me)$_2$), 3.49 (bs, 1H, BDI C*H*(Me)$_2$), 1.61-1.51 (m, 9H, BDI CH(*Me*)$_2$), 1.43-1.38 (m, 3H, BDI CH(*Me*)$_2$), 1.37-1.28 (m, 6H, BDI CH(*Me*)$_2$), 1.23 (bs, 6H, BDI CH(*Me*)$_2$), 1.12 (s, 3H, HC[*Me*C(NAr)]$_2$), 1.11 (s, 3H, HC[*Me*C(NAr)]$_2$), -5.07 (s, 1H, Re-H).^{13}C NMR for **2-CO** (151 MHz, C_6D_6, 298 K): 214.33 (XylN*C*), 164.53 (HC[Me*C*(NAr)]$_2$), 163.68 (HC[Me*C*(NAr)]$_2$), 154.89 (BDI Ar), 151.69 (BDI Ar), 144.58 (BDI Ar), 142.19 (BDI Ar), 141.99 (BDI Ar), 140.90 (BDI Ar), 125.68 (BDI Ar), 125.49 (BDI Ar), 124.93 (BDI Ar), 122.96 (BDI Ar), 122.58 (BDI Ar), 101.30 (H*C*[MeC(NAr)]$_2$), 83.05 (Cp), 28.35 (BDI *C*H(Me)$_2$), 27.50 (BDI *C*H(Me)$_2$), 25.14 (BDI CH(*Me*)$_2$), 24.82 (BDI CH(*Me*)$_2$), 24.24 (BDI CH(*Me*)$_2$), 23.50 (BDI CH(*Me*)$_2$), 23.23 (BDI CH(*Me*)$_2$), 23.07 (BDI CH(*Me*)$_2$), 21.57 (HC[*Me*C(NAr)]$_2$). FT-IR (Nujol): 1774 cm^{-1} (CO). Anal. Calcd. for $ReC_{35}H_{47}N_2O$ (**1-CO**): C, 60.21; H, 6.79; N, 4.01 %. Found: C, 60.45; H, 6.97; N, 4.13 %.

(XylNC)Re(η^5-Cp)(BDI-H) (1-XylNC)

Na[Re(η^5-Cp)(BDI)] (50 mg, 0.072 mmol) was dissolved in THF (2 mL) and this solution was set to stir. Separately, 2,6-xylylisocyanide (9.5 mg, 0.072 mmol) was dissolved in THF and this solution was added by pipette to the stirred solution of rhenium compound, giving a dark orange/brown solution. After 2 minutes, triethylammonium tetraphenylborate (30 mg, 0.072 mmol) was dissolved in THF (3 mL) and added to the reaction mixture, giving a bright red solution. After stirring the reaction mixture for 15 additional minutes at room temperature, its volatile components were removed in vacuo. The residue was extracted with hexane (5 mL), and these extracts were filtered through Celite before their volatile components were removed in vacuo to give an oily residue. This residue was dissolved in HMDSO (1 mL) with minimal agitation and allowed to sit at ambient temperature overnight, leading to the formation of dark red crystals of **1-XylNC** (44 mg, 76%). m.p.: 173-178 °C melting with decomp. ^{1}H NMR for **2-XylNC** (600 MHz, C_6D_6, 298 K): 7.14-7.02 (m, 6H, BDI Ar), 7.00 (d, 2H, *J* = 7.5, XylNC Ar), 6.87 (t, 1H, *J* = 7.5 Hz, XylNC Ar), 4.75 (s, 1H, *H*C[MeC(NAr)]$_2$), 4.18 (s, 5H, Cp), 3.80 (bs, 3H, BDI C*H*(Me)$_2$), 3.60 (bs, 1H, BDI C*H*(Me)$_2$), 2.46 (s, 6H, XylNC Me), 1.64 (bs, 3H, HC[*Me*C(NAr)]$_2$), 1.58 (bs, 3H, HC[*Me*C(NAr)]$_2$), 1.53 (bs, 3H, BDI CH(*Me*)$_2$), 1.41 (bs, 3H, BDI CH(*Me*)$_2$), 1.39 (bs, 3H, BDI CH(*Me*)$_2$), 1.19 (bs, 9H, BDI CH(*Me*)$_2$), 1.09 (bs, 3H, BDI CH(*Me*)$_2$), 0.93 (bs, 3H, BDI CH(*Me*)$_2$), -5.59 (s, 1H, Re-H).^{13}C NMR for **2-XylNC** (151 MHz, C_6D_6, 298 K): 192.43 (XylN*C*), 163.80 (HC[Me*C*(NAr)]$_2$), 162.71 (HC[Me*C*(NAr)]$_2$), 155.43 (BDI Ar), 152.61 (BDI Ar), 143.10 (BDI Ar), 142.18 (BDI Ar), 141.57 (BDI Ar), 135.83 (XylNC Ar), 133.00 (XylNC Ar), 125.62 (BDI and XylNC Ar), 125.03 (BDI Ar), 124.12 (XylNC Ar), 123.42 (BDI Ar), 122.96 (BDI Ar), 101.37 (H*C*[MeC(NAr)]$_2$), 81.72 (Cp), 28.71 (BDI *C*H(Me)$_2$), 27.53 (BDI *C*H(Me)$_2$), 25.62 (BDI CH(*Me*)$_2$), 25.21 (BDI CH(*Me*)$_2$), 24.67 (BDI CH(*Me*)$_2$), 24.23 (BDI CH(*Me*)$_2$), 23.87 (BDI CH(*Me*)$_2$), 22.30 (HC[*Me*C(NAr)]$_2$), 19.48 (XylNC Me). FT-IR (Nujol): 1931 cm^{-1} (XylNC). Anal. Calcd. for $ReC_{43}H_{56}N_3$ (**1-XylNC**): C, 64.45; H, 7.05; N, 5.25 %. Found: C, 64.46; H, 7.12; N, 5.29 %.

(N$_2$)Re(η^5-Cp)(BDI-H) (1-N$_2$)

Solutions of Na[Re(η^5-Cp)(BDI)] (50 mg, 0.072 mmol) and 2,6-di-*tert*-butylphenol (15 mg, 0.072 mmol) in Et_2O (5 mL and 1.5 mL, respectively) were prepared and cooled to -78 °C in the cold well of the glovebox. The 2,6-di-*tert*-butylphenol solution was added rapidly to the other, with brief physical agitation to mix. An immediate color change to dark orange-red was observed, concurrently with the formation of red crystals. The reaction mixture was allowed to sit in the cold well without agitation for 30 min. The red crystalline precipitate was then isolated and washed with cold (-78 °C) Et_2O (2 x 2 mL), followed by quick washes with room temperature Et_2O (3 x 1 mL). Removal of residual volatiles in vacuo yielded **1-N$_2$** as red crystals (31 mg, 61%). m.p.: 116-121 °C. ^{1}H NMR (700 MHz, C_6D_6, 298 K): 7.10 (d, 2H, *J* = 7.4 Hz, BDI Ar), 7.01 (d, 2H, *J* = 7.4 Hz, BDI Ar), 6.97 (t, 2H, *J* = 7.5 Hz, BDI Ar), 3.96 (s, 5H, Cp), 3.43 (sept, 2H, *J* = 6.8 Hz, BDI-H C*H*(CH$_3$)$_2$), 3.06 (d, 1H, *J* = 17.3 Hz, BDI-H CH$_2$), 2.92 (sept, 2H, *J* = 6.8 Hz, BDI-H C*H*(CH$_3$)$_2$), 2.56 (d, 1H, *J* = 17.3 Hz, BDI-H CH$_2$), 1.39 (s, 6H, H$_2$C[*Me*C(NAr)]$_2$), 1.36 (d, 6H, *J* = 6.6 Hz, BDI-H CH(C*H$_3$*)$_2$), 1.25 (d, 6H, *J* = 6.9 Hz, BDI-H CH(C*H$_3$*)$_2$), 1.20 (d, 6H, *J* = 6.7 Hz, BDI-H CH(C*H$_3$*)$_2$), 0.98 (d, 6H, *J* = 6.8 Hz, BDI-H CH(C*H$_3$*)$_2$). ^{13}C NMR (176 MHz, C_6D_6, 298 K): 175.33 (H$_2$C[Me*C*(NAr)]$_2$), 171.67 (BDI-H Ar), 140.60 (BDI-H Ar), 136.25 (BDI-H Ar), 126.02 (BDI-H Ar), 124.51 (BDI-H Ar), 122.61 (BDI-H Ar), 78.55 (Cp), 48.85 (H$_2$*C*[MeC(NAr)]$_2$), 27.98 (BDI-H *C*H(CH$_3$)$_2$), 27.68 (BDI-H *C*H(CH$_3$)$_2$), 27.08 (H$_2$C[*Me*C(NAr)]$_2$), 25.30 (BDI-H CH(*C*H$_3$)$_2$), 24.50 (BDI-H CH(*C*H$_3$)$_2$), 24.38 (BDI-H CH(*C*H$_3$)$_2$), 24.14 (BDI-H CH(*C*H$_3$)$_2$). FT-IR (Nujol): 1928 cm^{-1} (N$_2$). Anal. Calcd. for $ReC_{34}H_{47}N_4$ (**1-N$_2$**): C, 58.51; H, 6.79; N, 8.03 %. Found: C, 57.50; H, 6.47; N, 6.81%. The low combustion values for C and N in isolated **1-N$_2$** indicate the presence of impurities, likely a combination of Re(H)(η^5-Cp)(BDI) and Na[2,6-di-*tert*-butylphenolate]. The purity of isolated **1-N$_2$** is

sufficient to establish its identity, and we have found generating this material with other proton sources (such as $[Et_3NH][BPh_4]$ or $[(Et_2O)_2H]\{B[C_6H_3\text{-}3,5\text{-}(CF_3)_2]_4\}$) either leads to no precipitation of **1-N$_2$**, or the isolation of material with significantly lower purity.

$(C_6F_5)_3B(OC)Re(\eta^5\text{-}Cp)(BDI\text{-}H)$ (1-CO-B$(C_6F_5)_3$)

A solid mixture of **1-CO** (7 mg, 0.01 mmol) and $B(C_6F_5)_3$ (5 mg, 0.01 mmol) was dissolved in C_6D_6, yielding a bright orange solution. The resulting species was characterized by ^{1}H NMR spectroscopy and assigned to be the metal carbonyl borane adduct **1-CO-B$(C_6F_5)_3$** by virtue of its C_{2v} solution symmetry and ready similarity of its spectral data to that of **1-N$_2$**. ^{1}H NMR (700 MHz, C_6D_6, 298 K): 6.94-6.91 (m, 4H, BDI Ar), 6.84-6.81 (m, 2H, BDI Ar), 4.52 (d, 1H, *J* = 15.1 Hz, BDI-H CH_2), 4.23 (s, 5H, Cp), 3.50 (d, 1H, *J* = 15.2 Hz, BDI-H CH_2), 3.12 (sept, 2H, *J* = 6.7 Hz, BDI-H C*H*$(CH_3)_2$), 2.26 (sept, 2H, *J* = 6.7 Hz, BDI-H C*H*$(CH_3)_2$), 1.57 (s, 6H, $H_2C[MeC(NAr)]_2$), 1.05 (d, 6H, *J* = 6.4 Hz, BDI-H CH(C*H*$_3)_2$), 1.04 (d, 6H, *J* = 6.6 Hz, BDI-H CH(C*H*$_3)_2$), 0.91 (d, 6H, *J* = 6.1 Hz, BDI-H CH(C*H*$_3)_2$), 0.69 (d, 6H, *J* = 6.7 Hz, BDI-H CH(C*H*$_3)_2$).

NMR Spectra

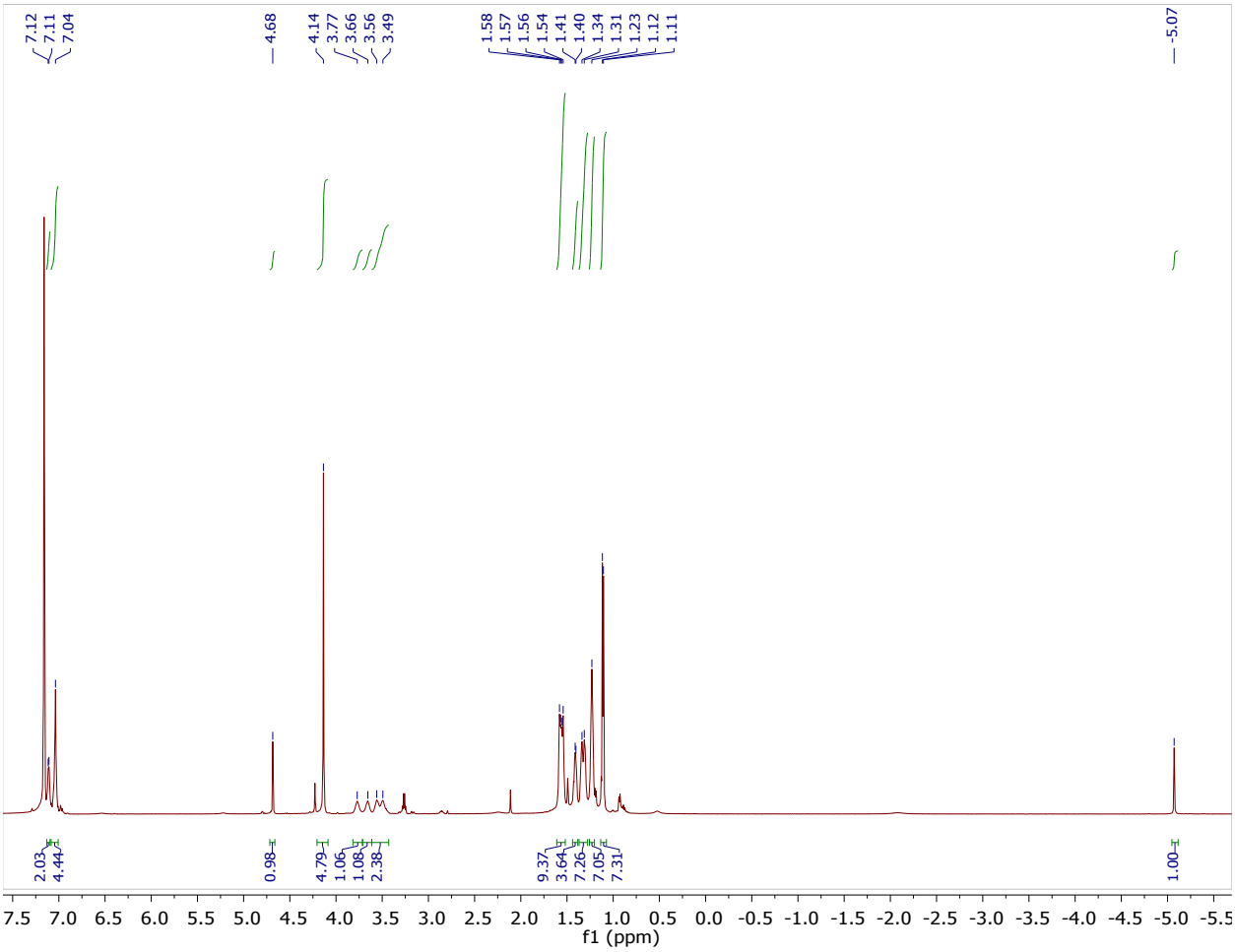

Figure S1. ^{1}H NMR Spectrum of **2-CO** in C_6D_6.

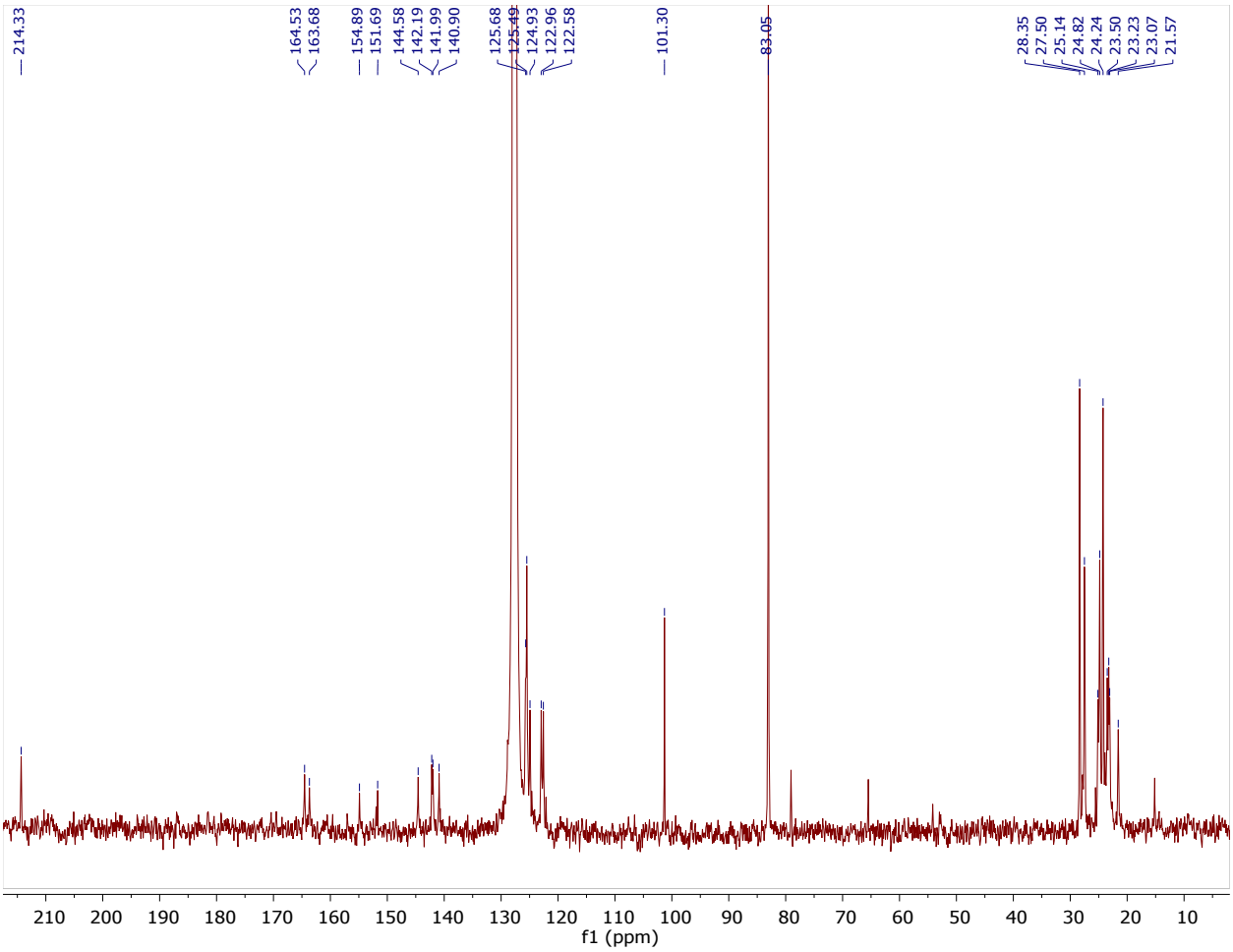

Figure S2. ^{13}C NMR Spectrum of **2-CO** in C_6D_6. A line broadening filter of 10 Hz has been applied to distinguish select, broad peaks.

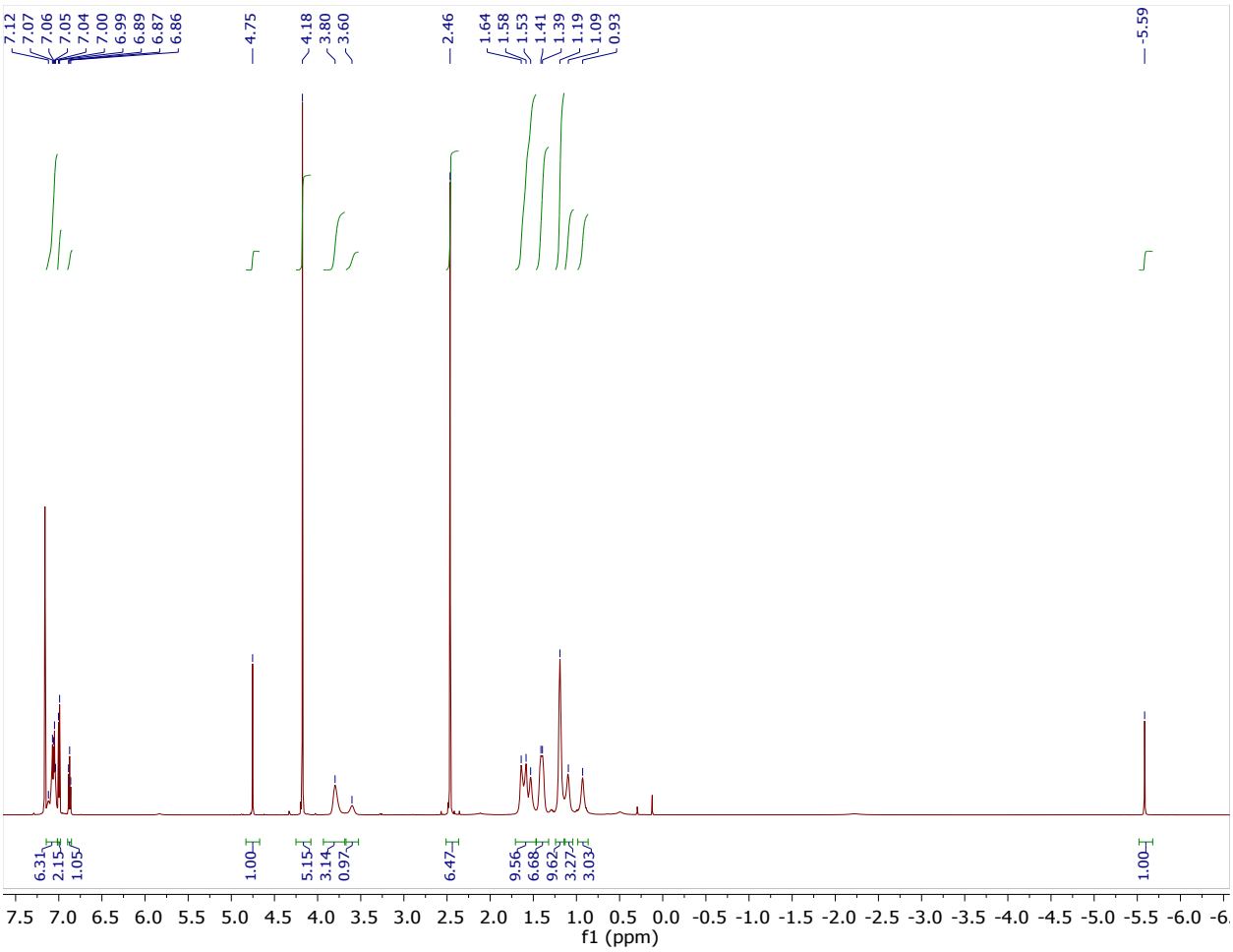

Figure S3. ^{1}H NMR Spectrum of **2-XylNC** in C_6D_6.

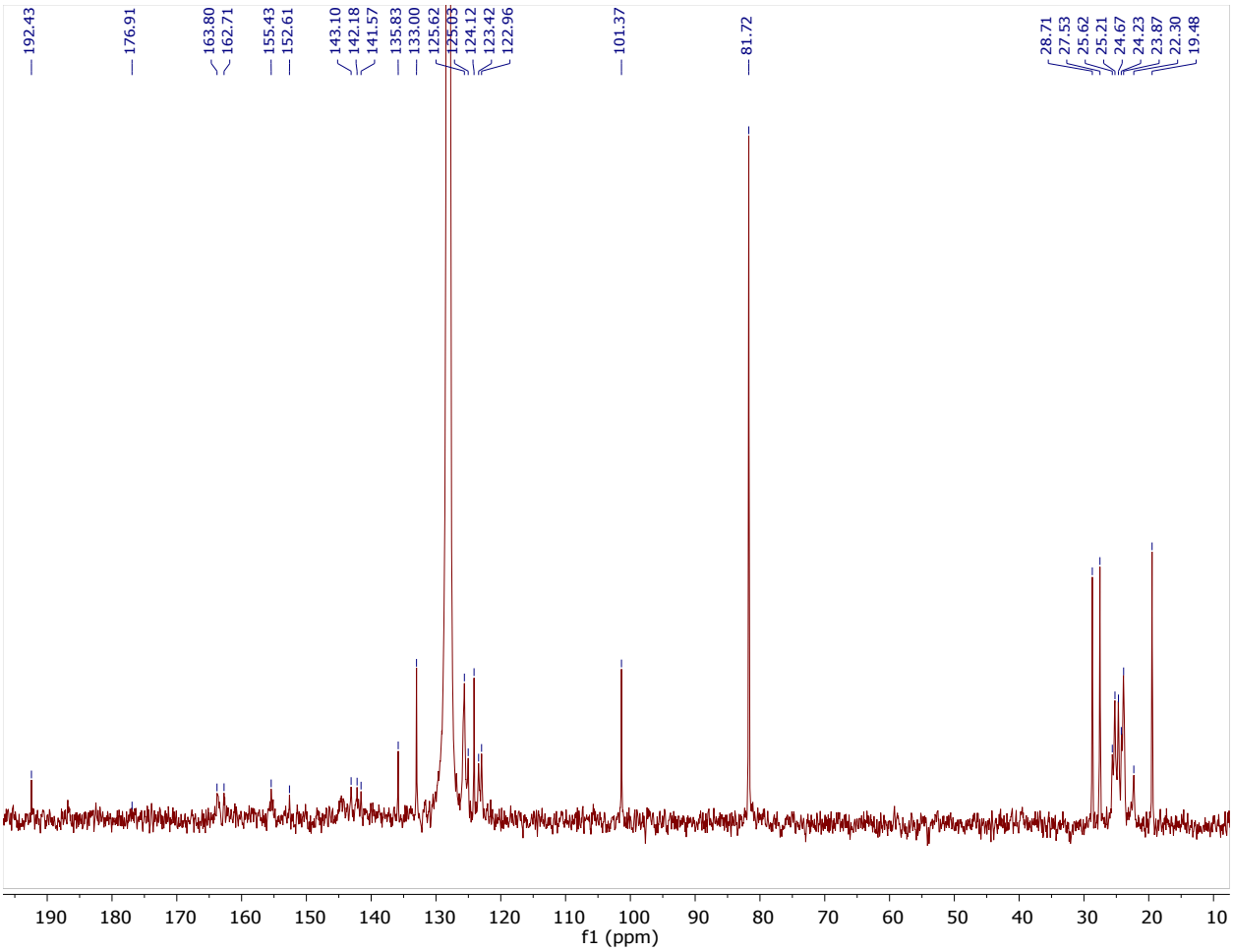

Figure S4. ^{13}C NMR Spectrum of **2-XylNC** in C_6D_6. A line broadening filter of 10 Hz has been applied to distinguish select, broad peaks.

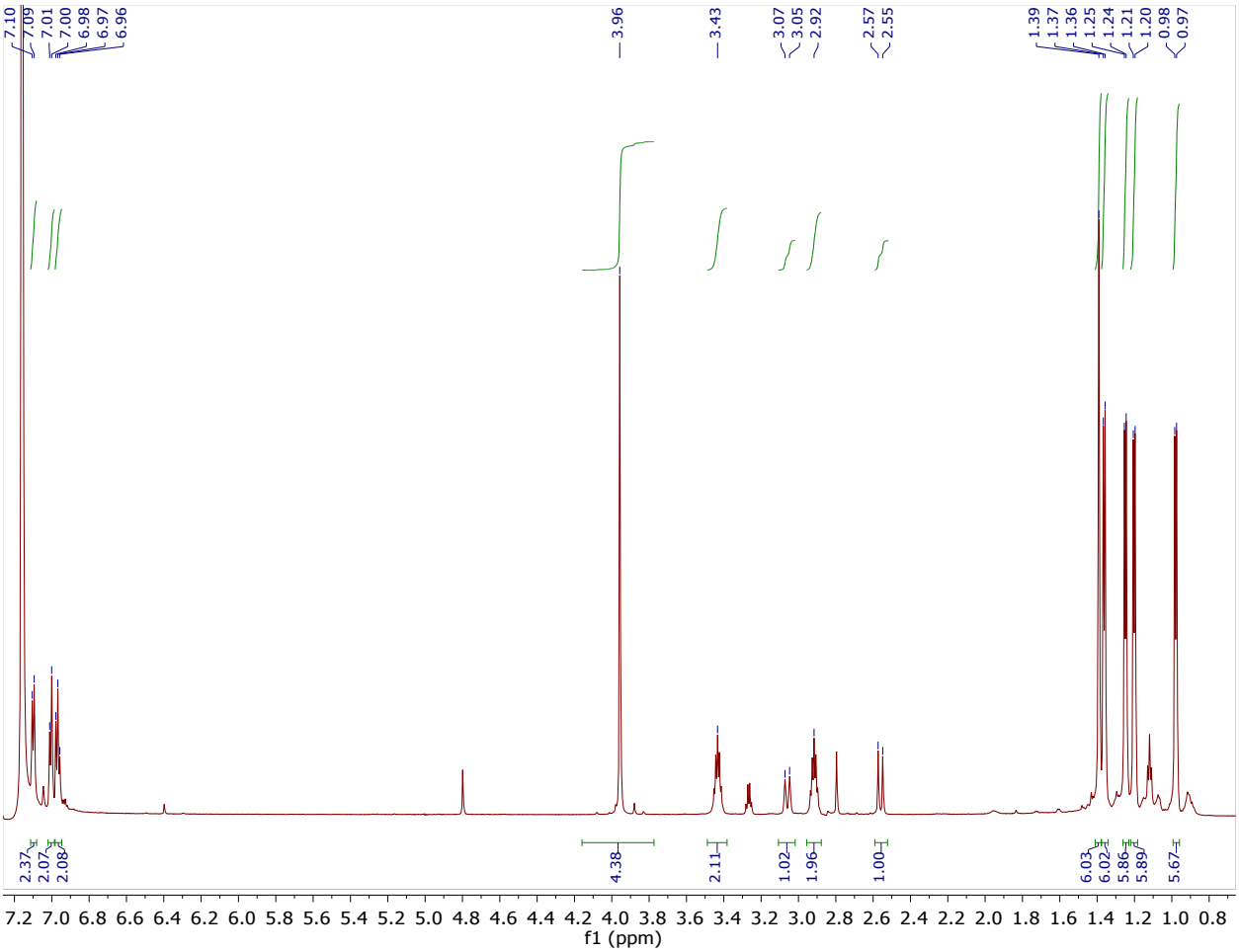

Figure S5. ^{1}H NMR Spectrum of **1-N_2** in C_6D_6. The hydride complex Re(H)(η^5-Cp)(BDI) is present as an impurity.

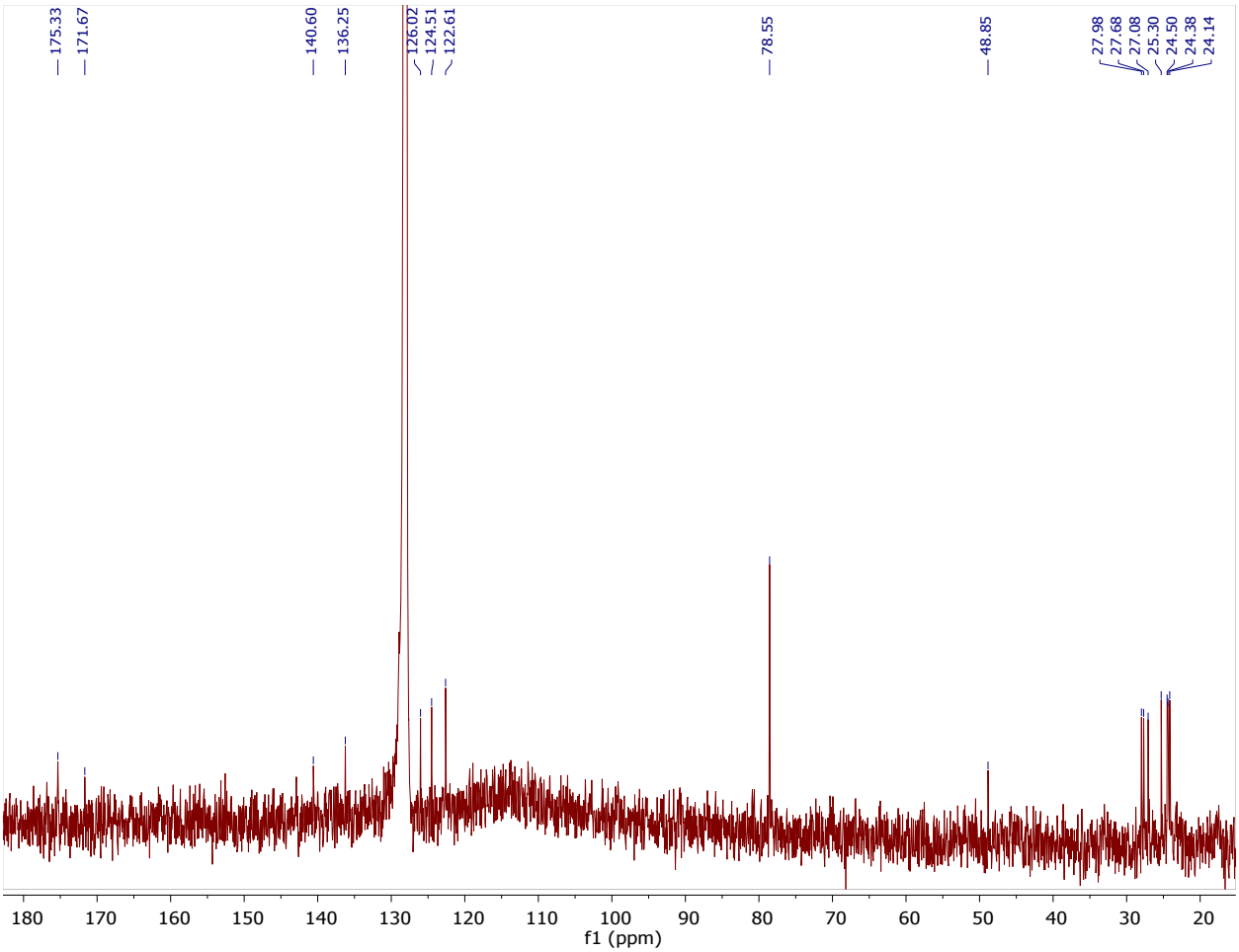

Figure S6. ^{13}C NMR Spectrum of **1-N_2** in C_6D_6.

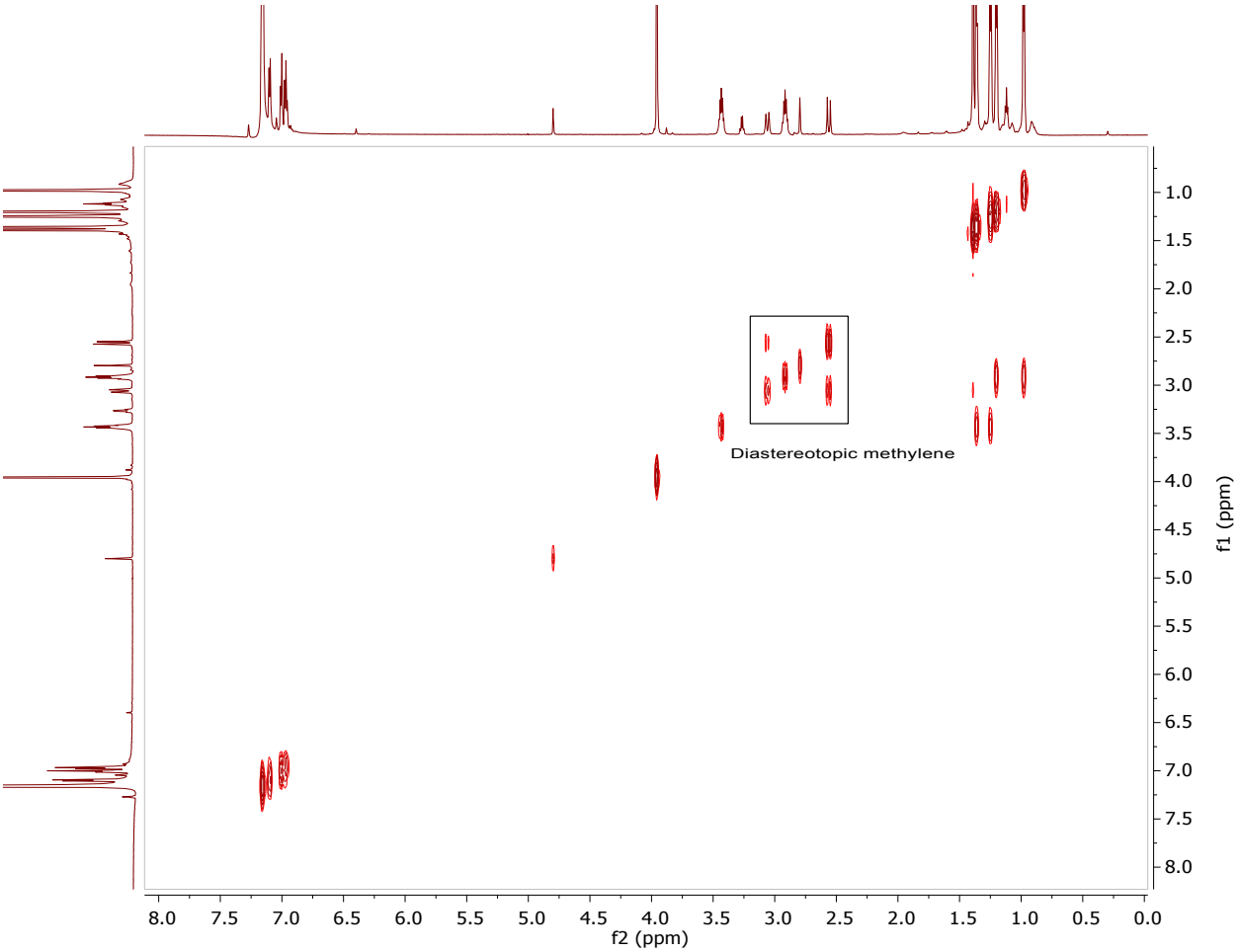

Figure S7. ^{1}H-^{1}H COSY Spectrum of **1-N_2** in C_6D_6, featuring the cross peaks for the diastereotopic methylene group of the BDI-H ligand.

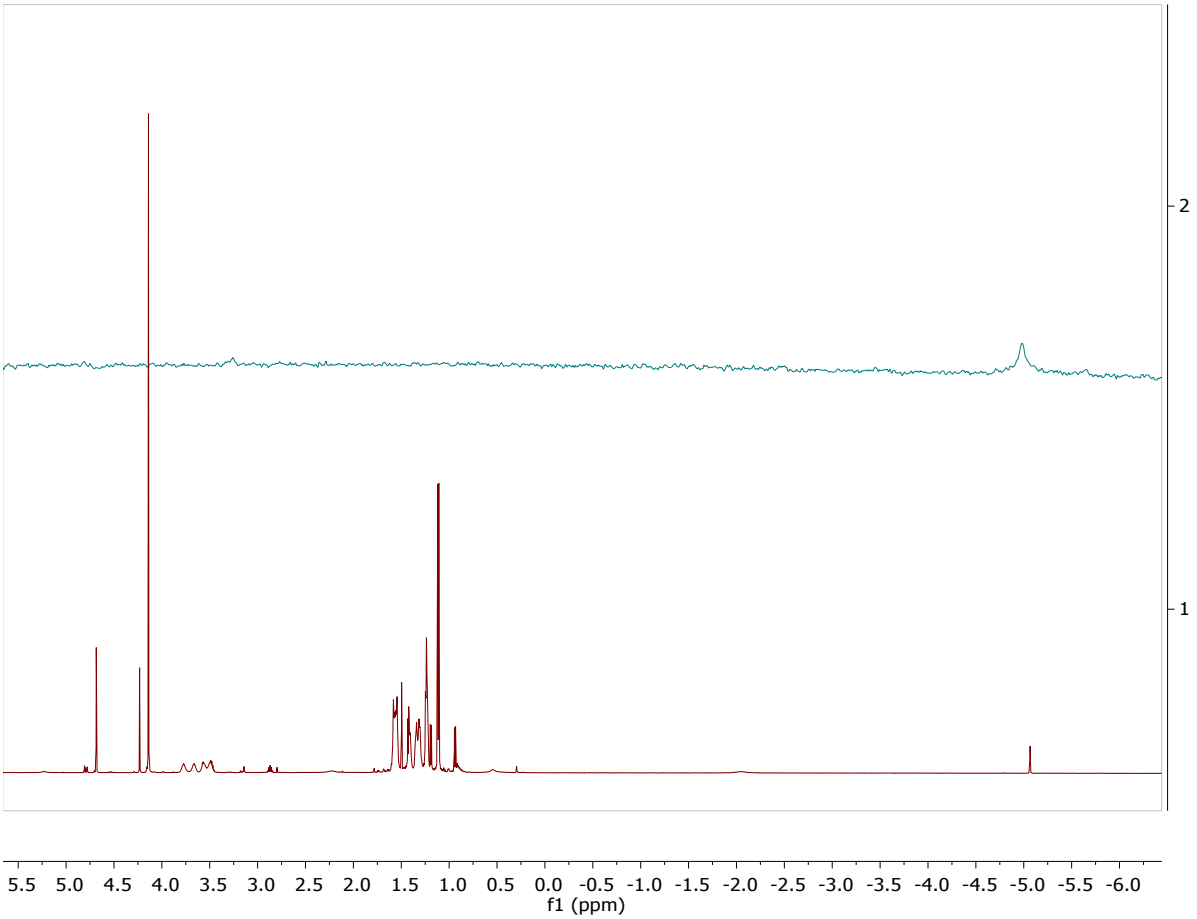

Figure S8. Sections of ^{1}H (bottom) and ^{2}H (top) NMR spectra of **2-CO** generated using $[Et_3ND][BPh_4]$, demonstrating main incorporation of deuterium into the metal hydride site.

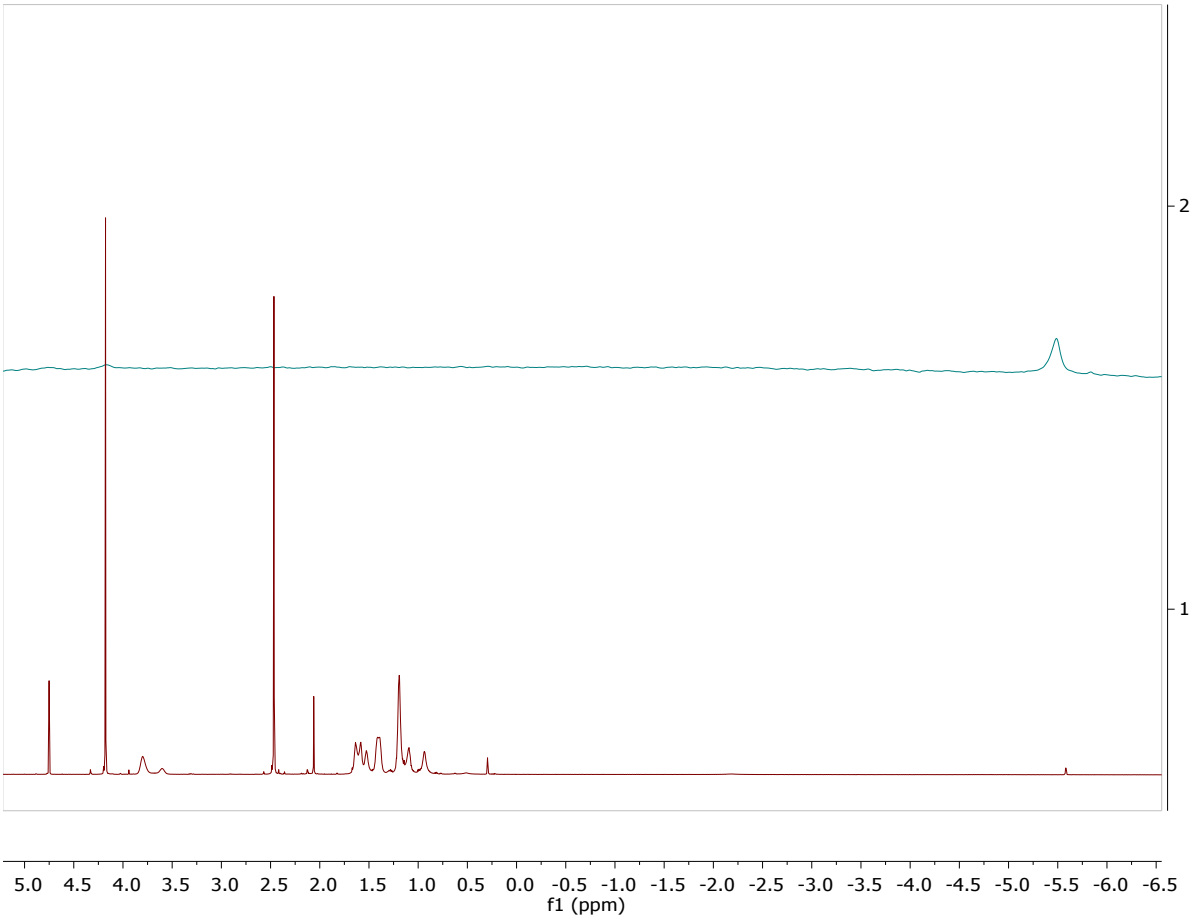

Figure S9. Sections of ^{1}H (bottom) and ^{2}H (top) NMR spectra of **2-XylNC** generated using $[Et_3ND][BPh_4]$, demonstrating main incorporation of deuterium into the metal hydride site.

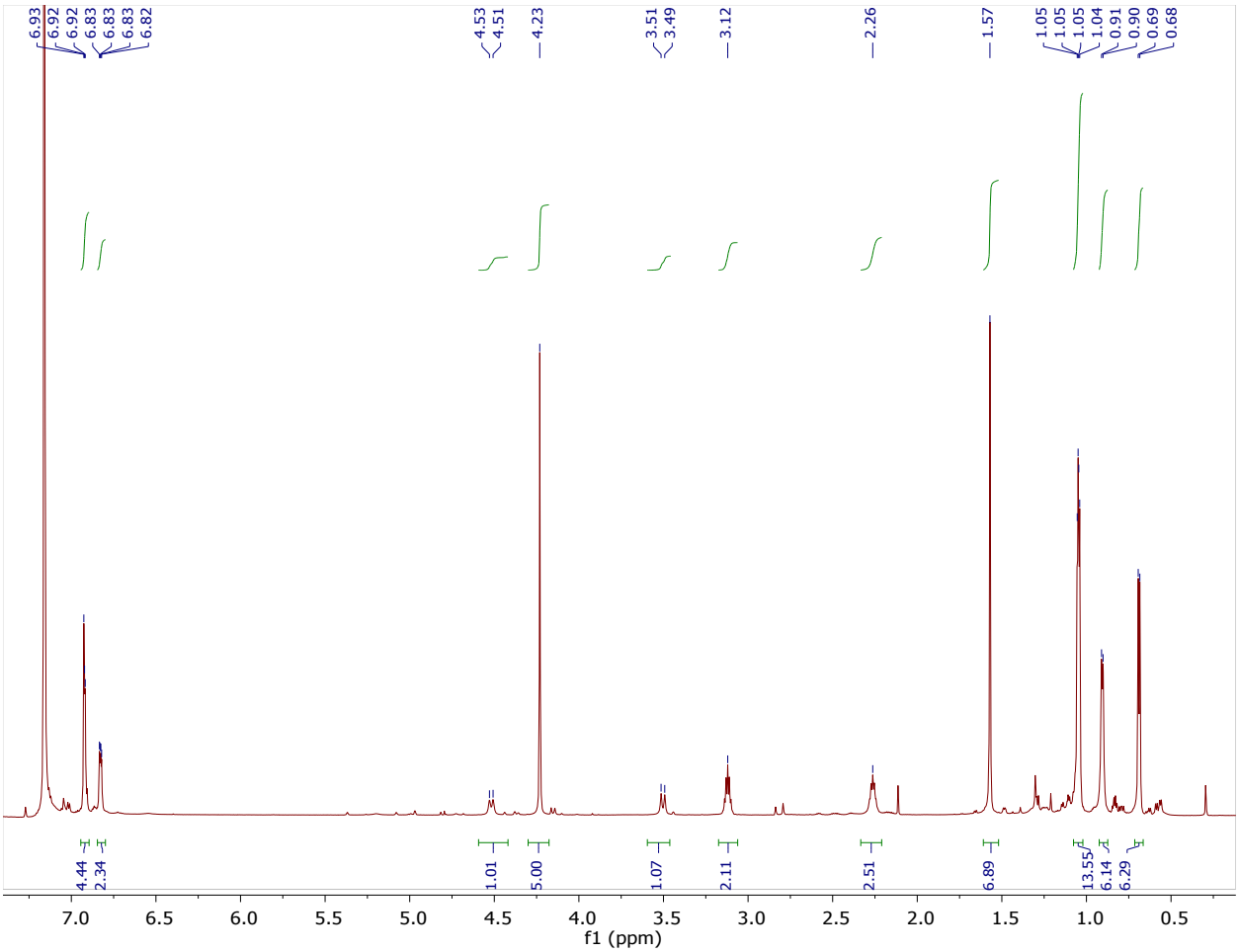

Figure S10. ^{1}H NMR spectrum of **1-CO-B(C_6F_5)$_3$**. Note the presence of broad, diastereotopic methylene resonances.

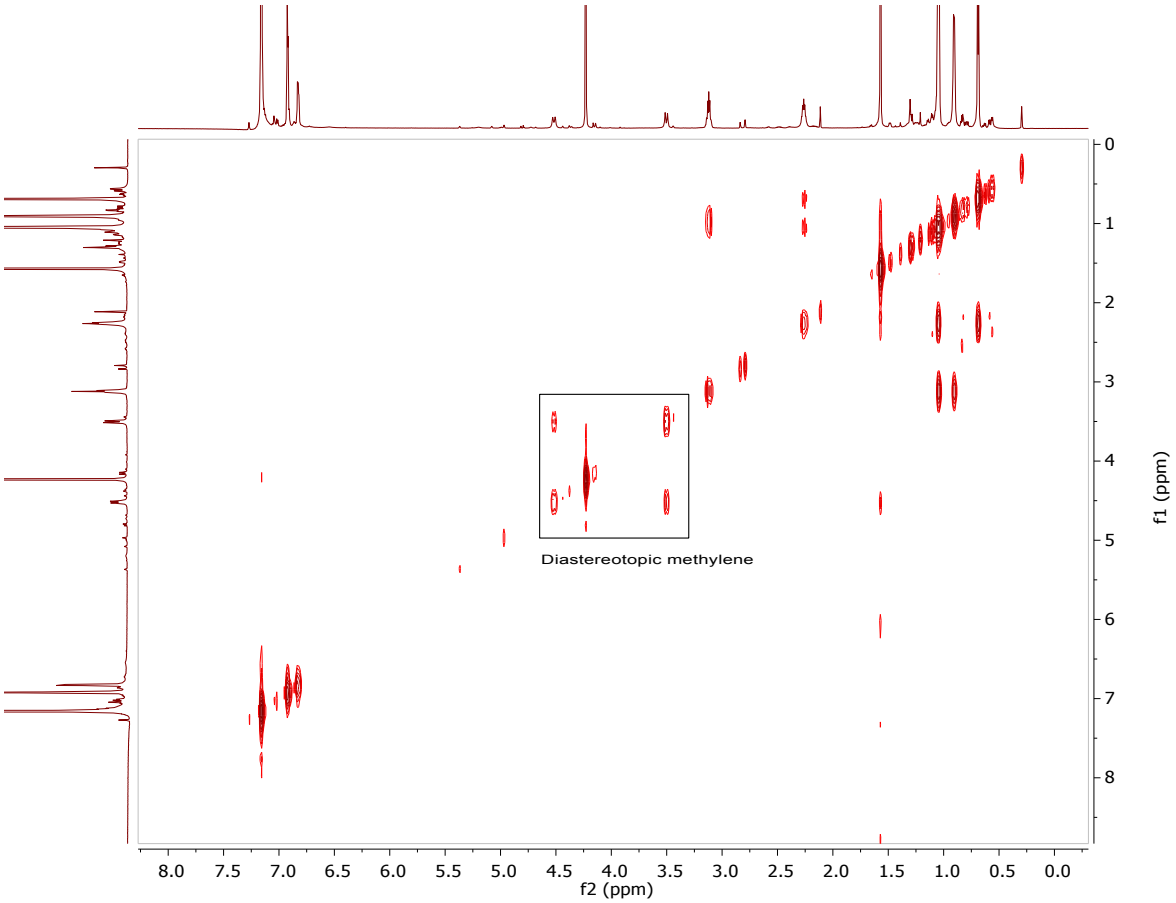

Figure S11. ^{1}H-^{1}H COSY spectrum of **1-CO-B(C_6F_5)$_3$**. Note the presence of a cross peak between the diastereotopic methylene resonances noted in the previous figure.

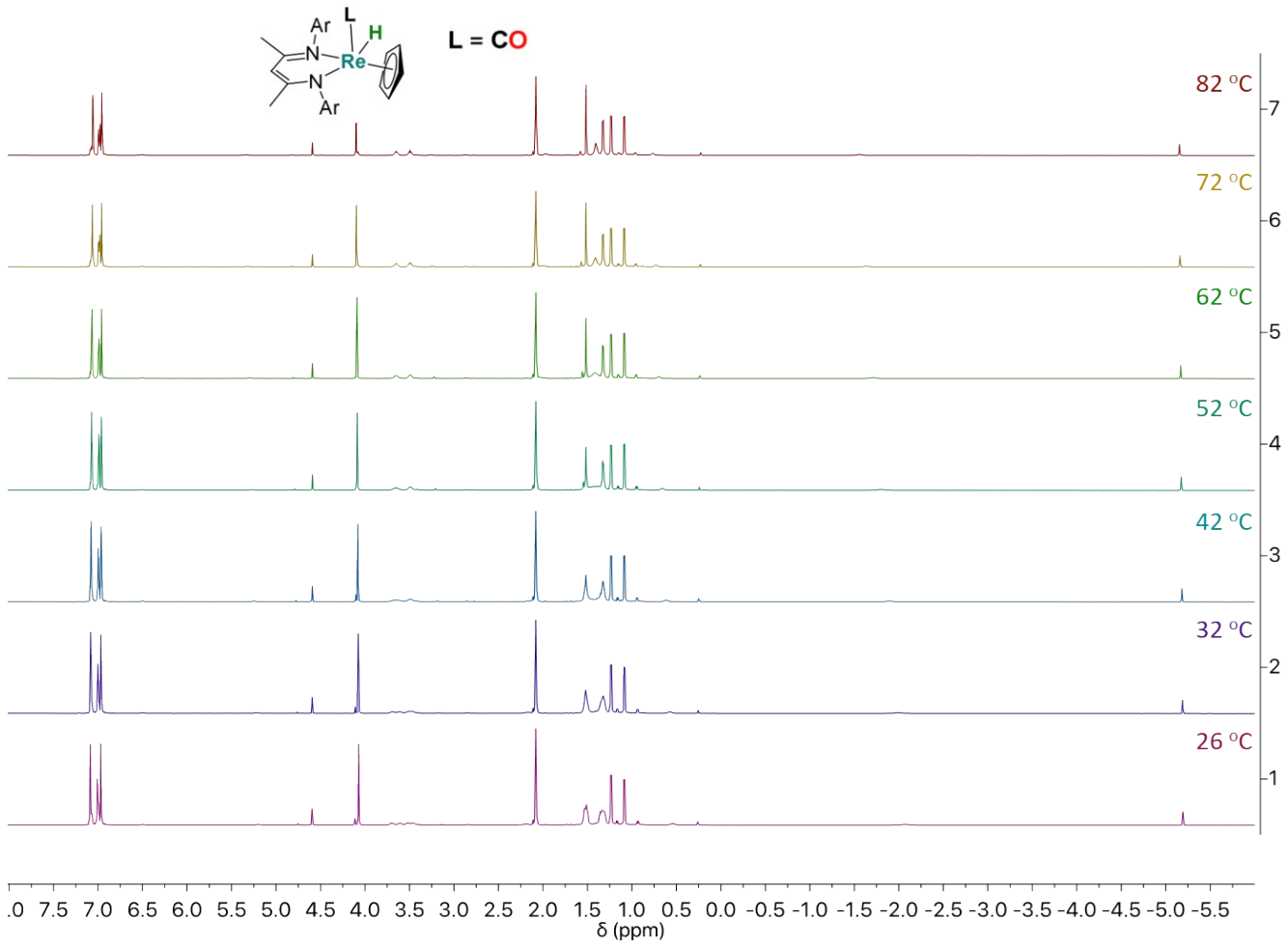

Figure S12. Variable temperature ^{1}H NMR spectra of **2-CO** in toluene-d8.

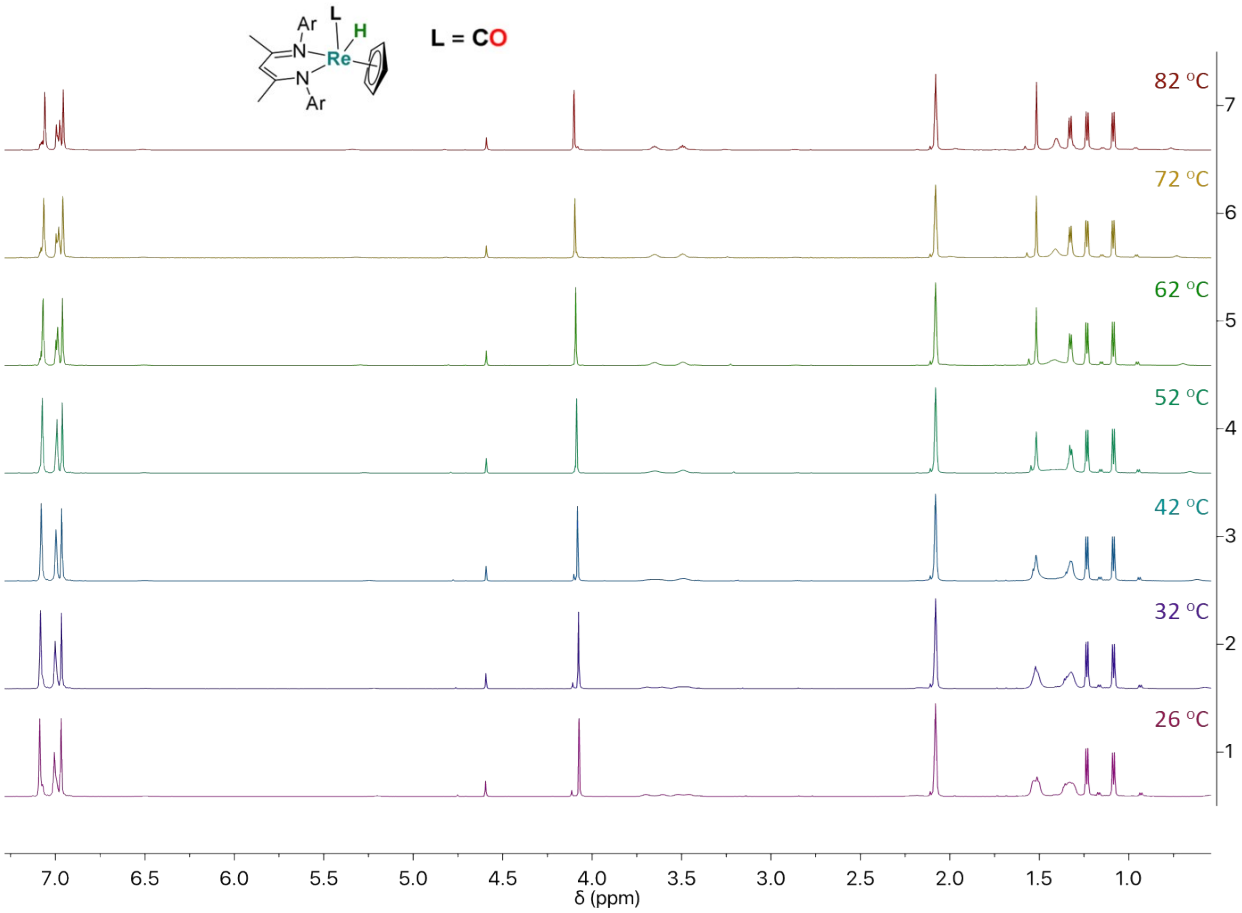

Figure S13. Variable temperature ^{1}H NMR spectra of **2-CO** in toluene-d8, focused on the non-hydride resonances.

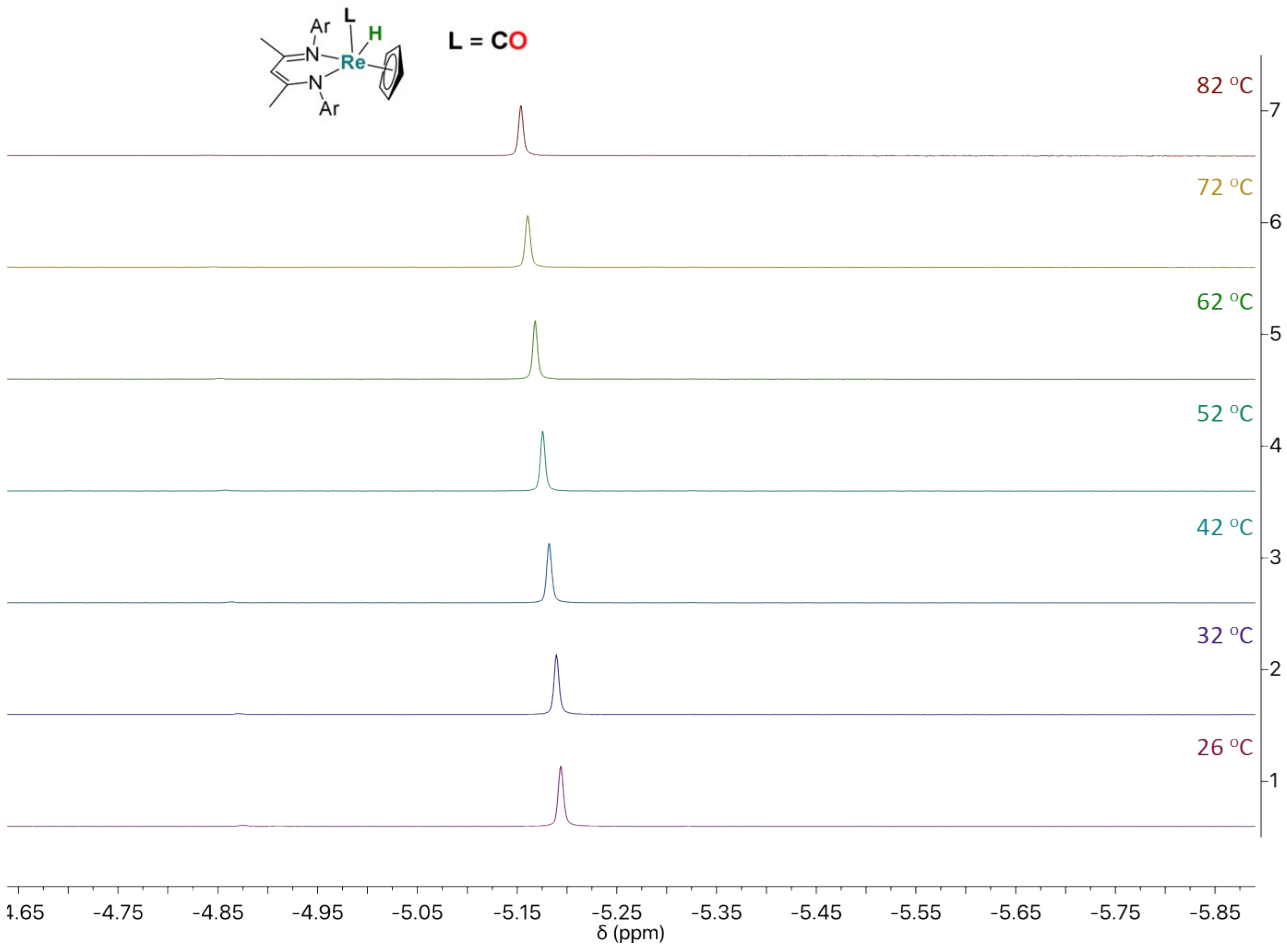

Figure S14. Variable temperature ^{1}H NMR spectra of **2-CO** in toluene-d8, focused on the hydride resonance.

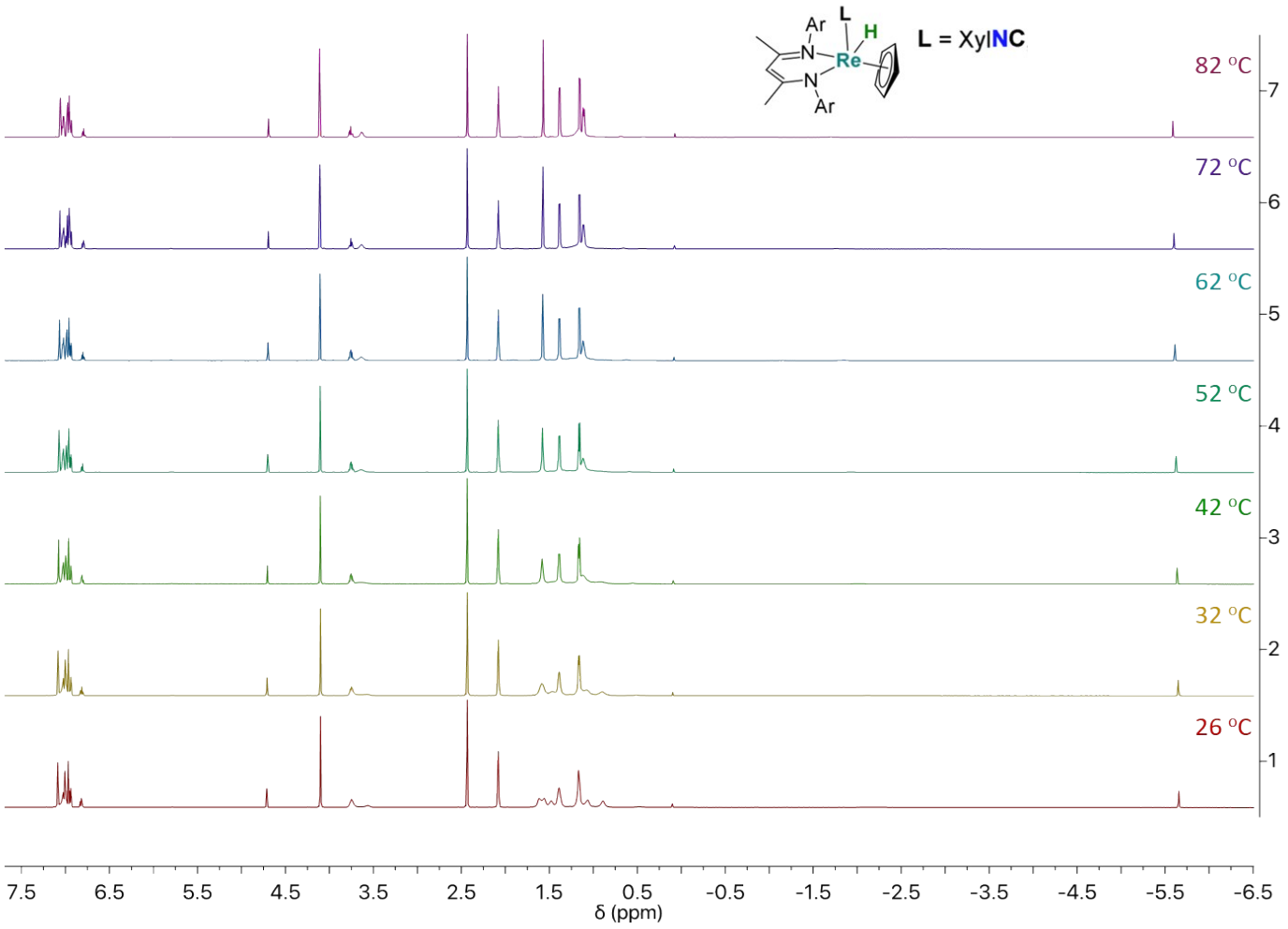

Figure S15. Variable temperature ^{1}H NMR spectra of **2-XylNC** in toluene-d8.

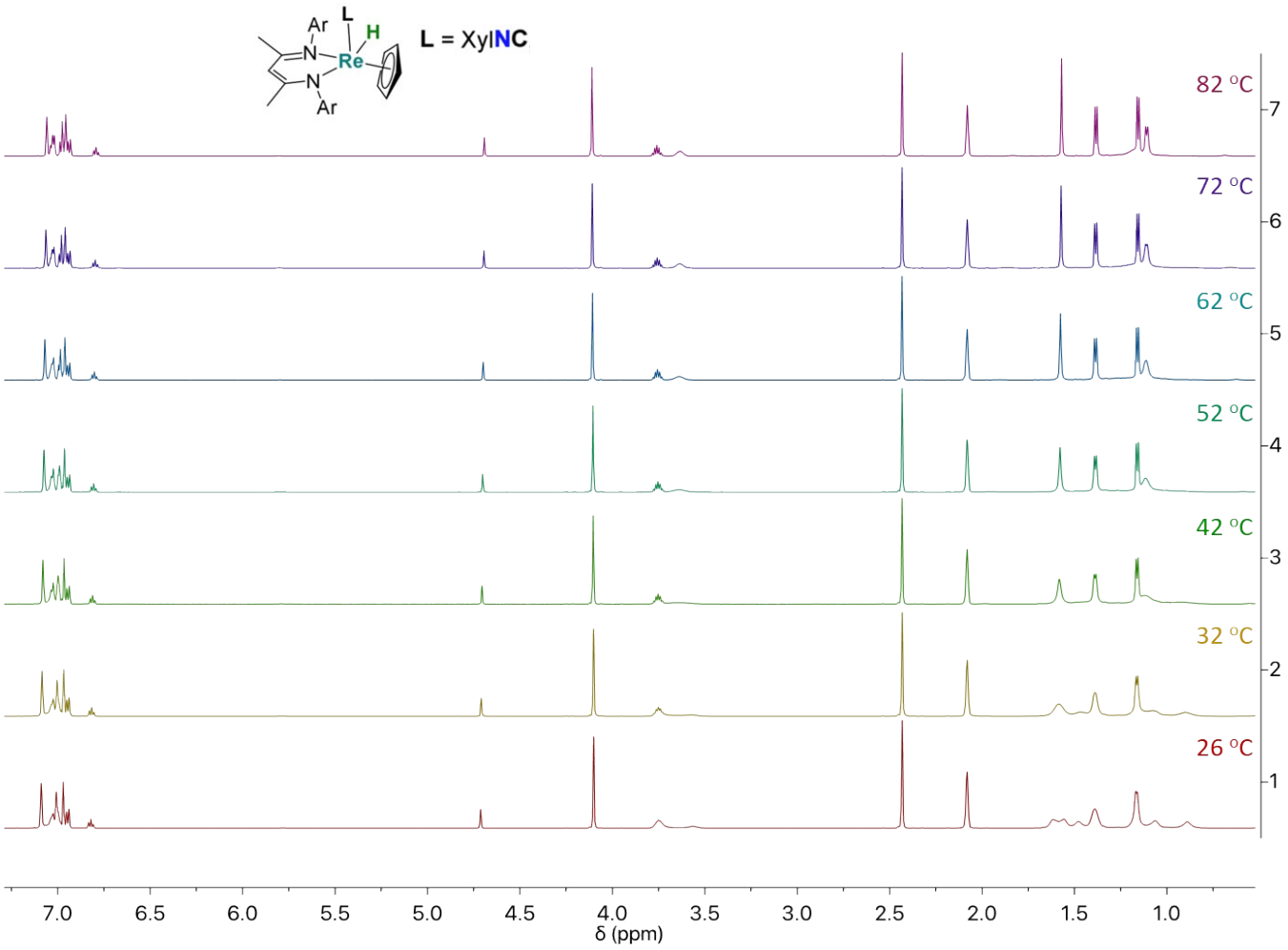

Figure S16. Variable temperature ^{1}H NMR spectra of **2-XylNC** in toluene-d8, focused on the non-hydride resonances.

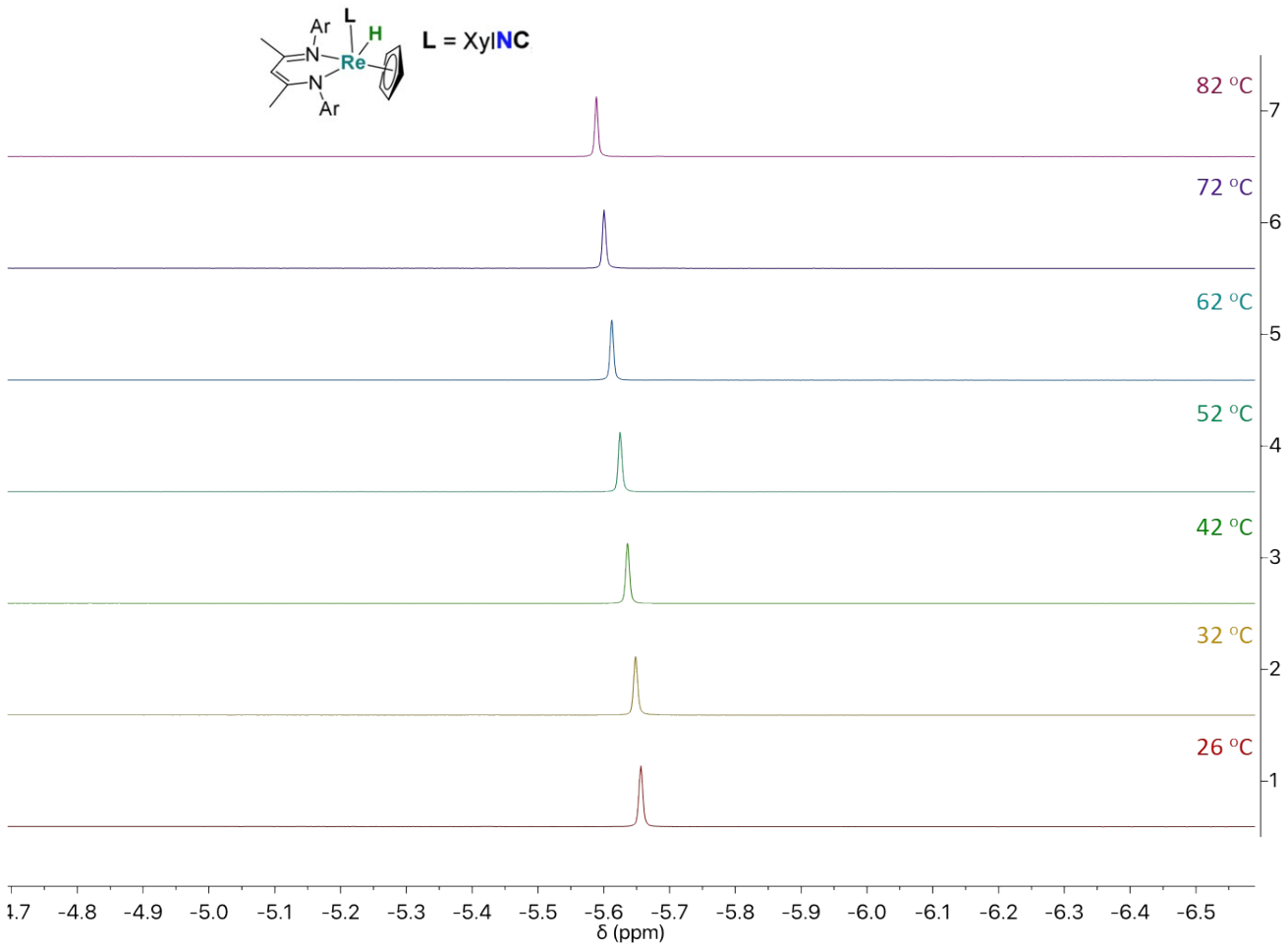

Figure S17. Variable temperature ^{1}H NMR spectra of **2-XylNC** in toluene-d8, focused on the hydride resonance.

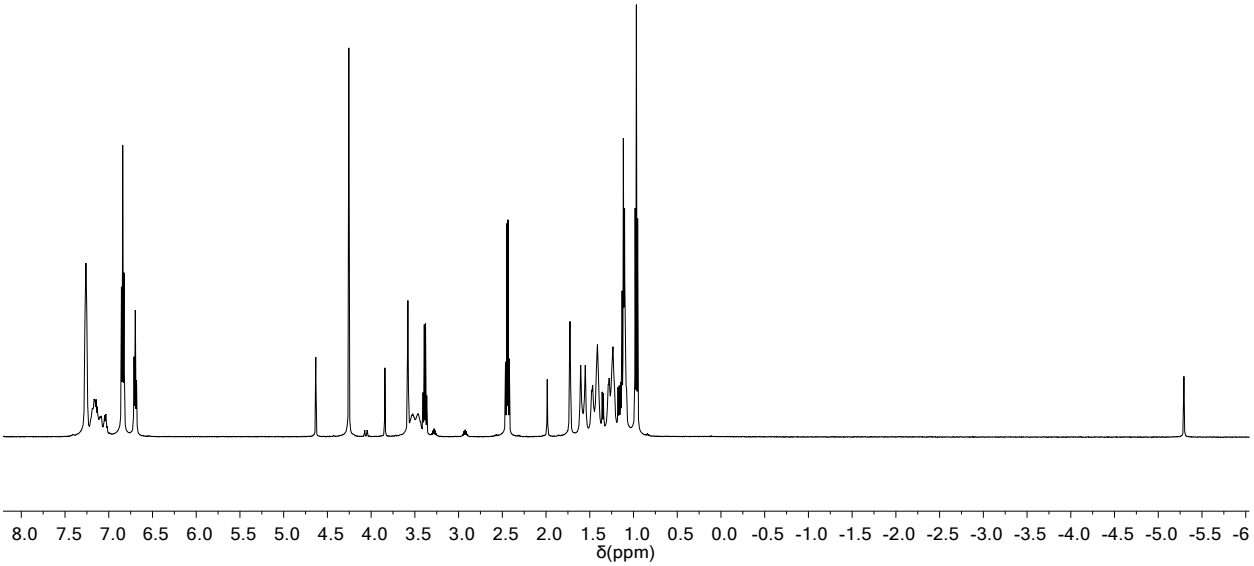

Figure S18. ^{1}H NMR spectrum of **2-CO** in THF-d8 as formed by the reaction between $\{(Et_2O)Na[(OC)Re(\eta^5\text{-}Cp)(BDI)]\}_2$ and triethylammonium tetraphenylborate.

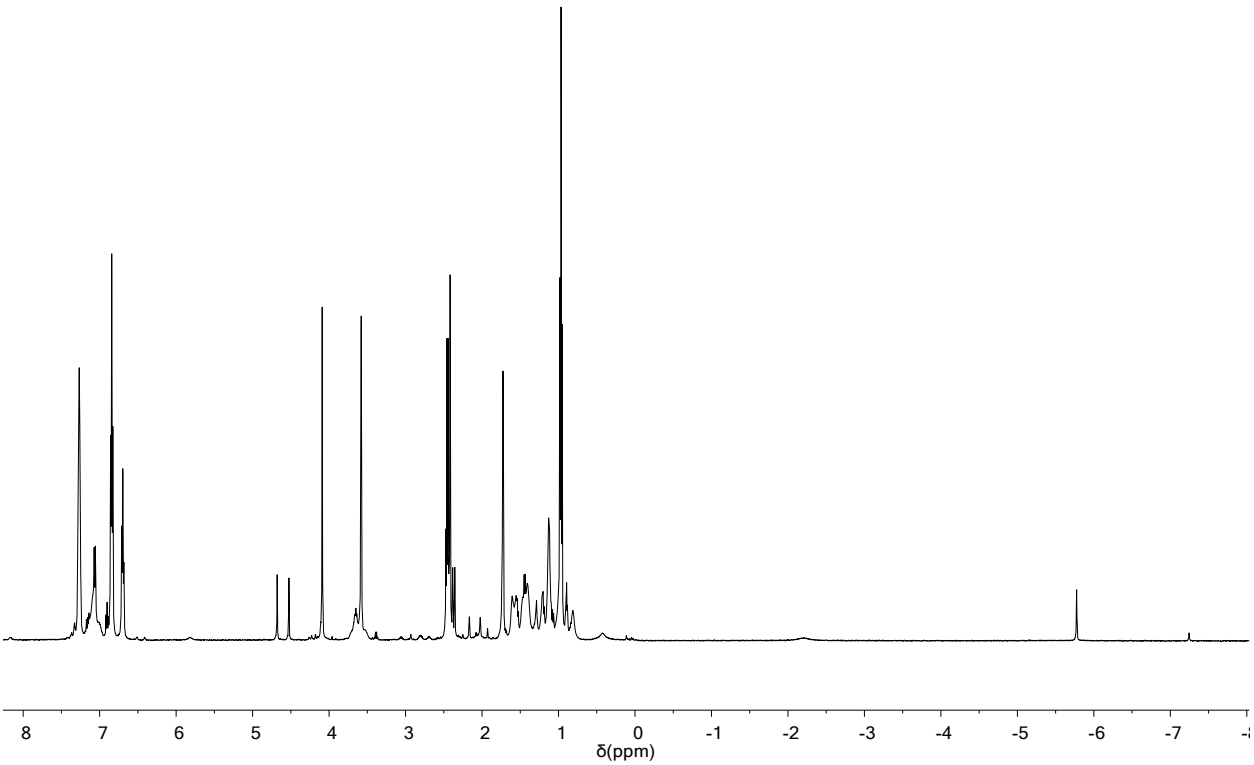

Figure S19. ^{1}H NMR spectrum of **2-XylNC** in THF-d8 as formed by the reaction between Na[Re(η^5-Cp)(BDI)], XylNC, and triethylammonium tetraphenylborate.

Crystallographic Tables and Information

X-ray diffraction data were collected at CheXray, UC Berkeley (**1-N_2**) and the Advanced Light Source (ALS) beamline 12.2.1, Lawrence Berkeley National Laboratory (**1-CO**, **1-XylNC**). At CheXray, measurements for **1-N_2** were taken using a Rigaku XtalLAB P200 instrument equipped with a rotating-anode Mo X-ray source and a Pilatus 200K detector, and the data was analyzed, reduced, and solved using the CrysAlisPro software package and Olex2 (SHELXT and SHELXL).[5,6,7] Measurements for **1-CO** and **1-XylNC** were taken at the ALS beam line 12.2.1, using a silicon-monochromated beam of 17 keV (0.7288 Å) synchrotron radiation and a Bruker D8 diffractometer equipped with a Bruker PHOTON II CPAD detector. Diffraction data collected at the ALS were analyzed and reduced using the Bruker APEX3 software package, and the structures were solved and refined using SHELXT and SHELXL-2014 as implemented by WinGX.[8,9] All structures were collected at 100 K in a stream of dry nitrogen. The crystal of **1-XylNC** that was analyzed displayed whole molecule disorder across the glide plane of the space group $P2_1/m$: accordingly all atoms, even those not located directly on the glide plane were refined at 0.50 occupancy to yield a final model that appears as a single rhenium center with two overlapping sets of the surrounding ligands. All structures have been deposited to the Cambridge Crystallographic Data Centre (CCDC), with deposition numbers 1943028 (**1-CO**), 1943029 (**1-XylNC**), 1943030 (**1-N_2**).

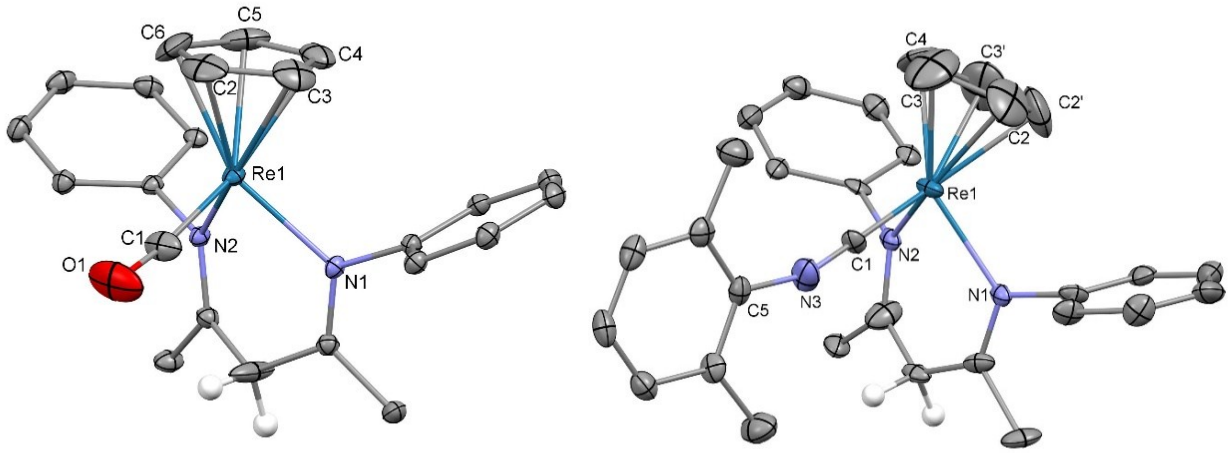

Figure S20. X-ray crystal structures of **1-CO** (left) and **1-XylNC** (right) with 50% probability ellipsoids. BDI isopropyl groups, hydrogen atoms (except for those on the BDI methylene group), and disordered groups (whole molecule disorder in **2**) have been omitted for clarity. Selected bond distances (Å) and angles (°) for **1**: Re1-C1 = 1.868(2), Re1-N1 = 2.153(2), Re1-N2 = 2.155(2), Re1-Cp(centroid) = 1.913(1), C1-O1 = 1.173(3), Re1-C1-O1 = 171.5(2). Selected bond distances (Å) and angles (°) for **2**: Re1-C1 = 1.878(9), Re1-N1 = 2.206(7), Re1-N2 = 2.189(9), Re1-Cp(centroid) = 1.916(5), C1-N3 = 1.17(4), Re1-C1-N3 = 179.1(2), C1-N3-C5 = 162(3).

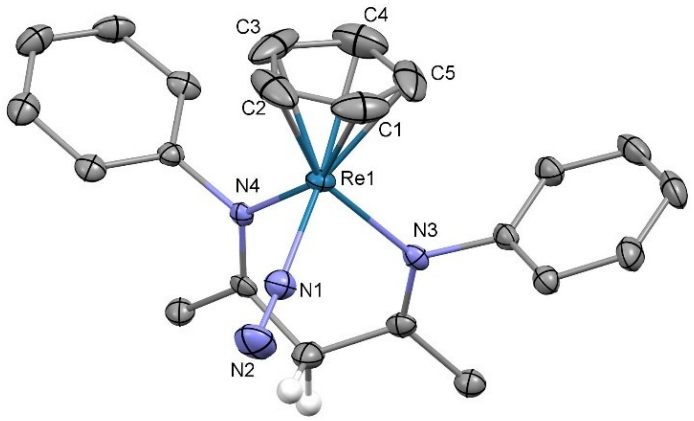

Figure S21. X-ray crystal structure of **1-N_2** with 50% probability ellipsoids. BDI isopropyl groups and hydrogen atoms (except for those on the BDI methylene group) have been omitted for clarity. Selected bond distances (Å) and angles (°): Re1-N1 = 1.938(4), Re1-N3 = 2.133(4), Re1-N4 = 2.124(4), Re1-Cp(centroid) = 1.876(3), N1-N2 =1.138(6) Re1-N1-N2 = 174.2(4).

Table S1. Crystallographic details and refinement metrics.

	1-CO	**1-XylNC**	1-N_2
Chemical formula	$C_{35}H_{47}N_2ORe$	$C_{43}H_{56}N_3Re$	$C_{34}H_{47}N_4Re$
Formula weight	697.94	801.10	1419.82
Color, habit	Red, rod	Red, tablet	Red, plate
Temperature (K)	100(2)	100(2)	100(2)
Crystal system	Monoclinic	Monoclinic	Monoclinic
Space group	$P2_1/n$	$P2_1/m$	$P2_1/n$
a (Å)	10.1864(3)	9.4458(5)	14.4071(5)
b (Å)	25.6639(9)	19.0455(10)	16.3244(5)
c (Å)	12.2342(4)	10.9694(6)	17.5429(5)
α (°)	90	90	90
β (°)	106.406(1)	106.664(2)	98.992(4)
γ (°)	90	90	90
V (Å^3)	3068.08(17)	1890.52(18)	3103.22(19)
Z	4	2	4
Density (Mg m^{-3})	1.511	1.407	1.494
F(000)	1416	820	1416
Radiation Type	Synchrotron	Synchrotron	MoK_α
μ (mm^{-1})	4.224	3.437	3.944
Crystal size (mm^3)	0.120 x 0.030 x 0.020	0.200 x 0.120 x 0.030	0.100 x 0.080 x 0.050
Meas. Refl.	56000	22975	34216
Indep. Refl.	9381	3566	5680
R(int)	0.0434	0.0445	0.0631
Completeness to arcsin(0.6*λ)	99.9%	99.5%	99.8%
Final R indices [I > 2σ(I)]	R = 0.0211 R_w = 0.0488	R = 0.0521 R_w = 0.1383	R = 0.0332 R_w = 0.0686
Goodness-of-fit	1.035	1.453	1.058
$\Delta\rho_{max}$, $\Delta\rho_{min}$ (e Å^{-3})	1.575, -1.313	1.406, -5.218	3.350, -1.996
Flack parameter	n/a	n/a	n/a

FT-IR Spectra

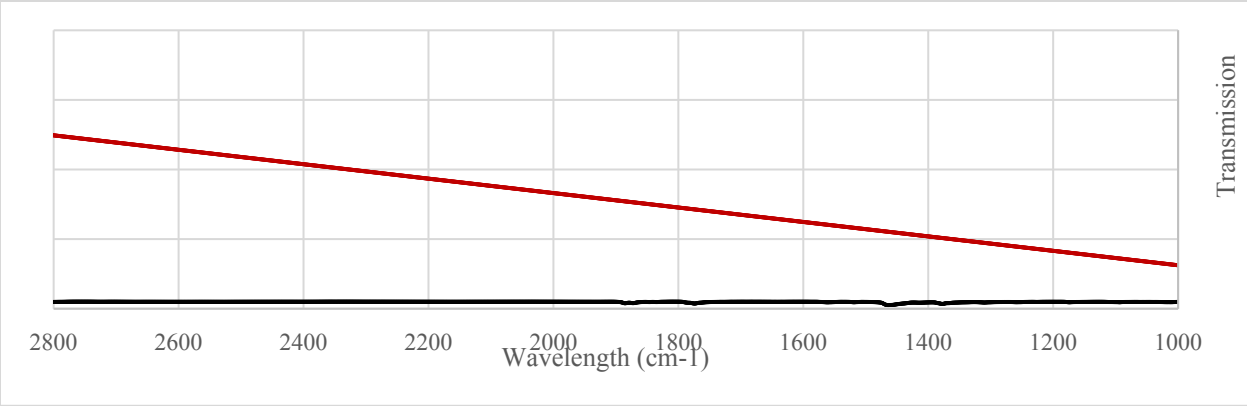

Figure S22. FT-IR absorbance spectrum of **1-CO** (Nujol/KBr).

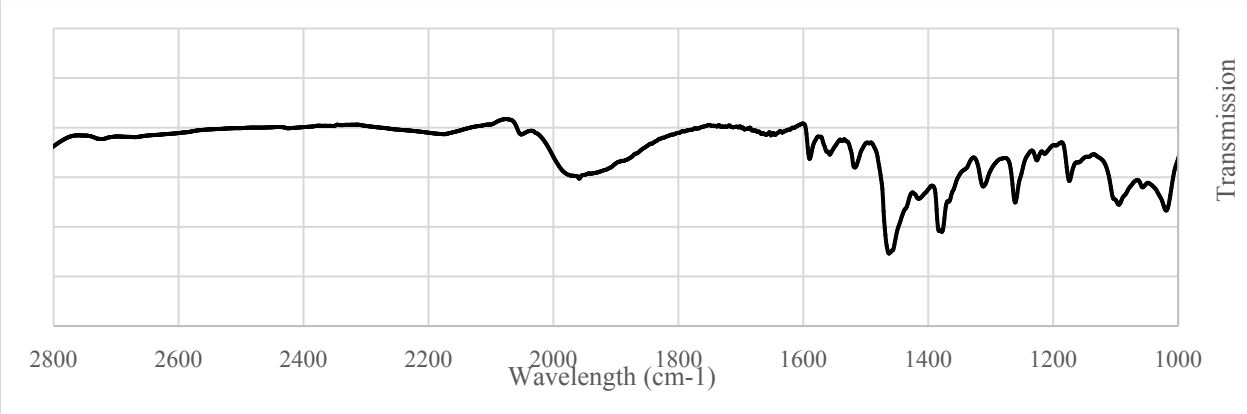

Figure 23. FT-IR absorbance spectrum of **1-XylNC** (Nujol/KBr).

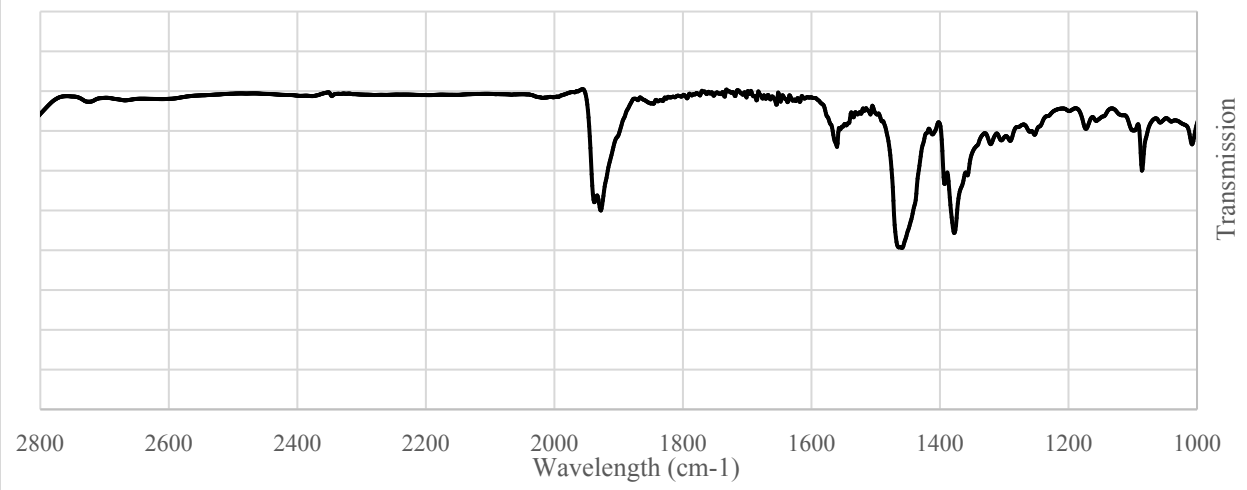

Figure S24. FT-IR absorbance spectrum of **1-N_2** (Nujol/KBr).

Computational Details and Results

Calculations were carried out with the *Gaussian16* program[10] employing the wB97XD functional,[11] which includes a version of Grimme's D2 model for dispersion effects.[12] The Re atoms were treated with the corresponding Stuttgart-Dresden RECP (relativistic effective core potential).[13] A mixed basis set was employed, as follows: def2-TZVPD FOR Re, def2-SVPD for N, C (for CO, XylNC, and sp^2 atoms in the BDI ligand), O (in CO), and H (for the H atom energy, metal hydride ligands, and H atoms at the BDI backbone).[14] For all the remaining atoms (sp^3 C atoms in the BDI and H atoms other than those specified above) the def2-SVDD basis set was used. Calculations were carried out without any symmetry restrictions. Structures were determined to be minima based on the absence of any imaginary vibrational modes. Coordinates of optimized structures may be found in the mol2 format, within the supplementary .zip file associated with this publication.

The calculation of Re-H and C-H BDFE values as discussed in the main text were done according to reported methods,[15] whereby the free gas phase energies of a series of H-atom donor/acceptor pairs are calculated (in this case employing wB97XD/def2-svpd) and used to obtain uncorrected element-H BDFE values. These uncorrected values are plotted against experimentally-determined gas phase BDFE values of the same compounds and a linear regression is performed, yielding a correction equation for element-H BDFE values obtained by the same computational methods (outlined in the paragraph above). The correction equation obtained for use in this study (as determined using the data in Table S2 and Figure S51) was BDFE(corrected) = 1.02*BDFE(uncorrected)-0.869 kcal/mol.

Table S2. Data employed to obtain a correction formula for calculated Re-H and C-H BDFE values as listed in Table S3. The E-H BDFE lit. values have been reported and used for this purpose previously.[15,16]

Compound	Energy (Hartrees)	E-H BDFE calc. (kcal/mol)	E-H BDFE lit. (kcal/mol)	Error (kcal/mol)
PhOH	-307.084611	77.4	79.8	-2.4
PhO	-306.448798			
$PhNH_2$	-287.229271	83.6	81.5	2.1
PhNH	-286.58346			
NH_3	-56.48883	98.7	99.4	-0.7
NH_2	-55.819022			
N_2H_2	-110.51916	54.8	52.6	2.2
N_2H	-109.919299			
O_2H	-150.758822	41.2	42.7	-1.5
O_2	-150.180588			
C_6H_6	-231.934642	102.8	104.7	-1.9
C_6H_5	-231.258297			
H	-0.512536			

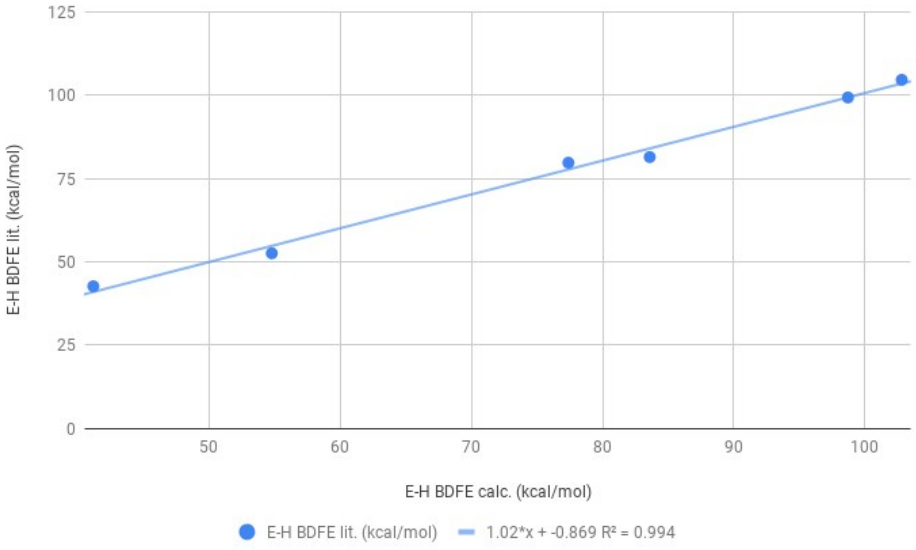

Figure S25. Plot of calculated vs. literature element-H BDFE values, and the corresponding linear regression (R^2 = 0.994) used as a correction equation for subsequent element-H BDFE calculations.

Table S3. Energies of DFT-Optimized Structures and Calculated Energy Differences and BDFE Values. L= N_2, CO, or XylNC, and H refers to the Re-H or BDI backbone C-H bond where appropriate. Corrected H BDFE values were obtained using the correction equation described above.

Compound	Energy (Hartrees)	Rel. Energy (kcal/mol)	L BDFE (kcal/mol)	H BDFE (kcal/mol)	Corrected H BDFE (kcal/mol)
cis **2-CO**	-1622.932284	-5.71	25.12	44.90	44.93
1-CO	-1622.923186	0	58.47	39.19	39.10
trans **2-CO**	-1622.911765	7.17	12.25	32.02	31.79
cis **2-XylNC**	-1912.27653	-7.92	30.02	45.29	45.33
1-XylNC	-1912.263913	0	61.16	37.38	37.26
trans **2-XylNC**	-1912.264848	-0.59	22.69	37.96	37.85
cis **2-N_2**	-1619.09189	-8.86	7.04	43.54	43.54
1-N_2	-1619.077773	0	23.17	34.68	34.50
trans **2-N_2**	-1619.091441	-8.58	7.32	43.25	43.25
(Cp)Re(CO)(BDI)	-1622.348199	n/a	34.42	n/a	n/a
(Cp)Re(XylNC)(BDI)	-1911.691812	n/a	38.92	n/a	n/a
(Cp)Re(N_2)(BDI)	-1618.509976	n/a	3.63	n/a	n/a
(Cp)Re(H)(BDI)	-1509.686826	0	n/a	54.20	54.41
(Cp)Re(BDI-H)	-1509.624582	39.06	n/a	15.14	14.57
(Cp)Re(BDI)	-1509.087919	n/a	n/a	n/a	n/a
CO	-113.205422	n/a	n/a	n/a	n/a
XylNC	-402.541863	n/a	n/a	n/a	n/a
N_2	-109.416275	n/a	n/a	n/a	n/a
H	-0.512536	n/a	n/a	n/a	n/a

References

1. Lohrey, T.D.; Maron, L.; Bergman, R.G.; Arnold, J. *J. Am. Chem. Soc.* **2019**, *141*, 800-804.
2. Lohrey, T.D.; Bergman, R.G.; Arnold, J. *Dalton Trans.* **2019**, *78*, DOI: 10.1039/C9DT04489B.
3. Kuuloja, N.M.; Kylmälä, T.M.; Tois, J.E.; Sjöholm, R.E.; Franzén, R.G. *Synthetic Communications* **2011**, *41*, 1052-1063.
4. Deaton, J.C.; Taliaferro, C.M.; Pitman, C.L.; Czerwieniec, R.; Jakubikova, E.; Miller, A.J.M.; Castellano, F.N. *Inorg. Chem.* **2018**, *57*, 15445-15461.
5. CrysAlisPro 1.171.39.45f (Rigaku Oxford Diffraction, 2018)
6. Dolomanov, O.V., Bourhis, L.J., Gildea, R.J, Howard, J.A.K. & Puschmann, H. (2009), J. Appl. Cryst. 42, 339-341.
7. Sheldrick, G.M. (2015). Acta Cryst. A71, 3-8.; Sheldrick, G.M. (2015). Acta Cryst. C71, 3-8.
8. *APEX2, APEX3, SADABS, and SAINT*. Bruker AXS. Madison, WI, USA.
9. Farrugia, L. J.; *J. Appl. Cryst.* **2012**, *45*, 849-854.
10. Gaussian 16, Revision B.01, Frisch, M. J.; Trucks, G. W.; Schlegel, H. B.; Scuseria, G. E.; Robb, M. A.; Cheeseman, J. R.; Scalmani, G.; Barone, V.; Petersson, G. A.; Nakatsuji, H.; Li, X.; Caricato, M.; Marenich, A. V.; Bloino, J.; Janesko, B. G.; Gomperts, R.; Mennucci, B.; Hratchian, H. P.; Ortiz, J. V.; Izmaylov, A. F.; Sonnenberg, J. L.; Williams-Young, D.; Ding, F.; Lipparini, F.; Egidi, F.; Goings, J.; Peng, B.; Petrone, A.; Henderson, T.; Ranasinghe, D.; Zakrzewski, V. G.; Gao, J.; Rega, N.; Zheng, G.; Liang, W.; Hada, M.; Ehara, M.; Toyota, K.; Fukuda, R.; Hasegawa, J.; Ishida, M.; Nakajima, T.; Honda, Y.; Kitao, O.; Nakai, H.; Vreven, T.; Throssell, K.; Montgomery, J. A., Jr.; Peralta, J. E.; Ogliaro, F.; Bearpark, M. J.; Heyd, J. J.; Brothers, E. N.; Kudin, K. N.; Staroverov, V. N.; Keith, T. A.; Kobayashi, R.; Normand, J.; Raghavachari, K.; Rendell, A. P.; Burant, J. C.; Iyengar, S. S.; Tomasi, J.; Cossi, M.; Millam, J. M.; Klene, M.; Adamo, C.; Cammi, R.; Ochterski, J. W.; Martin, R. L.; Morokuma, K.; Farkas, O.; Foresman, J. B.; Fox, D. J. Gaussian, Inc., Wallingford CT, 2016.
11. Chai, J.D.; Head-Gordon, M. *Phys. Chem. Chem. Phys.*, **2008**, *10*, 6615-6620.
12. Grimme, S.; Ehrlich, S.; Goerigk, L. *J. Comp. Chem.*, **2011**, *32*, 1456.
13. Andrae, D.; Haeussermann, U.; Dolg, M; Stoll, H.; Preuss, H. *Theor. Chim. Acta* **1990**, *77*, 123.
14. Rappoport, D.; Furche, F. *J. Chem. Phys.* **2010**, *133*, 134105.
15. Matson, B.D.; Peters, J.C. *ACS Catal.* **2018**, *8*, 1448-1455.
16. Warren, J.J.; Tronic, T.A.; Mayer, J.M. *Chem. Rev.* **2010**, *110*, 6961-7001.